Letter

Symmetry, superposition, and fragmentation in classical spin liquids: A general framework and applications to square kagome magnets

K. B. Yogendra, Suman Karmakar, and Tanmoy Das
Department of Physics, Indian Institute of Science, Bangalore 560012, India

(Received 18 March 2024; revised 4 June 2024; accepted 9 July 2024; published 1 August 2024)

Classical magnets exhibit exotic ground-state properties such as spin liquids and fractionalization, promising a manifestation of superposition and projective symmetry construction in classical theory. While system-specific spin-ice or soft-spin models exist, a formal theory for general classical magnets remains elusive. Here, we introduce a generic symmetry group construction built from a vector field in a plaquette of classical spins, demonstrating how classical spins superpose in irreducible representations (irreps) of the symmetry group. The corresponding probability amplitudes serve as order parameters and local spins as fragmented excitations. The formalism offers a many-body vector field representation of diverse ground states, including spin liquids and fragmented phases described as degenerate ensembles of irreps. We apply the theory to a frustrated square kagome lattice, where spin-ice or soft spin rules are inapt, to describe spin liquids and fragmented phases, all validated through irreps ensembles and unbiased Monte Carlo simulation. Our generic theory sheds light on previously unknown aspects of spin-liquid phases and fragmentation and broadens their applications to other branches of field theory.

DOI: 10.1103/PhysRevB.110.L060401

Introduction. Classical spin models can potentially capture exotic phenomena like spin liquid [1–6], spin ice [7–9], fragmentation [2,10–13], order by disorder [14–19], and prethermal discrete time crystals [20], and exciting progress lies in designing novel and generic frameworks [6,21–29]. While quantum theory allows the ground state of a spin liquid to be a superposition state, this concept does not have a classical analog. Classically, two main approaches so far describe the spin liquid phase. The spin ice model applies to specific spin Hamiltonians that can be expressed in terms of $|\mathbf{S}_c|^2$, where the total spin in a cluster c is as follows: $\mathbf{S}_c = \sum_{i\in c} \eta_i \mathbf{S}_i$, with η_i being suitably chosen rational numbers [6]. This way all possible $\mathbf{S}_c = 0$ microstates describe a degenerate ground state [2,3,6,11,23,24]. However, this rule does not hold for models with Dzyaloshinskii-Moriya (DM) interactions. Recently, a Luttinger-Tisza approximation, also known as the spherical or soft-spin approximation, has been employed to analyze the degenerate energy state in momentum space in terms of extended states of classical spin [23–27]. A flat band in this model indicates the degeneracy characteristic of spin liquids. The drawback of this model is that it relaxes the local $|\mathbf{S}_i| = 1$ constraint, imposing it at the global spin value. Both approaches are suited for specific Hamiltonians and have so far been applied only to spin-ice models.

Magnetic fragmentation is another exotic phenomenon in the classical spin systems that has drawn recent attention [10–13,30,31]. In this phase, a local classical field (such as spin or magnetization) fragments into components with one (or more) components exhibiting order while others remain disordered or liquidlike. This phenomenon has so far been studied using Landau's coarse-grained magnetization fields, with or without local spin constraints. Despite progress in understanding specific models with ground-state degeneracy or fragmentation, a comprehensive analytical framework, which would ideally encompass all lattice symmetries, frustration, DM interactions, and local spin constraints, and hence do not necessarily follow the spin-ice rule, remains elusive.

Research on frustrated lattices, like pyrochlore [6,32–37], triangular [38–40], kagome [41–43], and others [4,15,18, 44,45], has been a major focus in exploring spin liquids and related phenomena. Recently, the square kagome lattice has sparked excitement due to experimental hints of spin liquid phases [46–48] and supporting theoretical investigations [49–53]. However, these materials likely possess a strong DM interaction [46–48] which the spin-ice and soft-spin models do not incorporate. Additionally, the square kagome lattice boasts multiple sublattices, offering a richer platform with potentially larger degenerate manifolds and more fragmentation possibilities.

Here, we introduce a generic framework for studying ground-state degeneracy and fragmentation in classical spin systems using a group theory approach. Our approach transcends a prior approach [35,43], used primarily for ordered phases, to encompass spin liquids and fragmented phases. We define a vector space representing the spins within a lattice plaquette, designed to be invariant under the lattice's point-group symmetry. The plaquette spin vector can be expressed as a superposition of the irreducible representations (irreps) of the symmetry group. The expansion parameters of this superposition vector act as Landau-like order parameters. However, unlike traditional order parameters, they transform under "discrete" spatial rotations and acquire continuous symmetry through degeneracy and irreps multiplets. Interestingly, these order parameters serve as spins' "probability amplitudes" and "occupation densities" to irreps state and energy levels, respectively. This approach, with its resemblance to quantum concepts, paves the way for a novel construction of classical spin liquids and fragmentation states.

We apply the theory to a model consisting of XXZ and DM interactions in a two-dimensional (2D) square kagome lattice. We also employ unbiased classical Monte Carlo (MC) simulations to validate our group theory results and reproduce the phase diagram. We find that DM interactions promote a uniform or staggered ordering of specific irreps, containing a vortex or an antivortex. Near the critical boundaries between these ordered phases, we observe the emergence of classical spin liquid (CSL) states. Within the CSL phase, local spins remain fully disordered if the ground state consists of a randomly distributed irrep ensemble. Alternatively, the ground state can scramble ordered and disordered irreps to fragment the local spin vector into coexisting extended/collective and pointlike excitations. Additionally, the spin-spin correlation function is analyzed in each phase to distinguish between magnetic Bragg peaks for the collective excitations in the ordered phase and the "pinch-point" excitations in the liquid phases.

Mathematical foundation. We define a local vector field in a plaquette network p to be invariant under the lattice's point-group symmetry G:

$$\mathcal{S}_p = \bigoplus_{i\in p} S_i. \tag{1}$$

$S_i = (S_i^x\ S_i^y\ S_i^z)^T \in \mathsf{O}_i(3)$ at the ith site, and $\mathcal{S}_p \in \mathsf{O}_p(3n)$, where n is the number of sublattices in p. [$\mathsf{O}_i(n)$ and $\mathsf{O}_p(n)$ distinguish the orthogonal symmetry of the vector at the i site and the p plaquette, respectively]. Each plaquette, like a conventional unit cell, includes more sites than the primitive unit cell. This redundancy is adjusted by introducing a normalization factor in the dual vector definition to fix the length of $\mathcal{S}_p$ [55].

The transformation from the spin space to the irreps space of group G involves an orthogonal matrix, whose column vectors $\mathcal{V}_\alpha$ form the orthonormal basis of the irreps representation. Expressing $\mathcal{S}_p$ in this irrep space yields

$$\mathcal{S}_p = \sum_{\alpha=1}^{3n} m_\alpha \mathcal{V}_\alpha. \tag{2}$$

Here $m_\alpha \in \mathbb{R}$ are the coefficients of the expansions. We keep the plaquette index in m and $\mathcal{V}$ implicit for simplicity in notation. Interestingly, m_α conforms to Landau's order parameter as the coarse-grain average of local fields; except, here, it is invariant under a discrete symmetry group in a plaquette and is interpreted as the probability amplitude of the vector field: $m_\alpha = \mathcal{V}_\alpha^{\mathcal{T}} \mathcal{S}_p$ [55]. The local spins are defined by a rectangular projection matrix $\mathcal{P}_{i\in p}$ as $\mathbf{S}_{i\in p} = \mathcal{P}_{i\in p}\mathcal{S}_p = \sum_\alpha m_\alpha \mathcal{P}_{i\in p}\mathcal{V}_\alpha$.

Reformulating the order parameters in terms of the irreps conveniently decouples them in a symmetry-invariant Hamiltonian, albeit the irreps' multiples can mix among themselves. To account for the multiplets' submanifold and emergent symmetry, it is convenient to introduce an $\mathsf{O}_p(d_\alpha)$ "spinor-like" field, $\boldsymbol{m}_\alpha := (m_\alpha^{(1)} \dots m_\alpha^{(d_\alpha)})^T$, for the α irrep with d_α multiplets. Then, the eigenmodes are obtained by the orthogonal rotation $\tilde{\boldsymbol{m}}_\alpha = e^{i\boldsymbol{\mathcal{L}}_\alpha \cdot \boldsymbol{\phi}_\alpha} \boldsymbol{m}_\alpha$, where $\boldsymbol{\mathcal{L}}_\alpha$ are the corresponding generators for the angle $\boldsymbol{\phi}_\alpha$. $\boldsymbol{\phi}_\alpha$ lives on the Hamiltonian's parameter space and assumes fixed values for the energy eigenmodes. The orthonormal basis states ensure the constraint $|\mathcal{S}_p|^2 = \mathcal{S}_p^{\mathcal{T}}\mathcal{S}_p = \sum_\alpha d_\alpha |m_\alpha|^2 = nS^2, \forall p$, where $|S_i| = S$, is an additional hardcore constraint on the classical spins [55]. Not all irreps necessarily adhere to the local constraint, requiring them to collaborate with others for existence. Such irrep ensembles may lead to nonanalyticity and fragmentation into an order-disorder mixed phase.

We have the $3nN$-dimensional vector space $\mathcal{S} = \bigoplus_p \mathcal{S}_p$ for a generic N-unit cell lattice, commencing a $3nN \times 3nN$-matrix-valued quadratic-in-spin Hamiltonian (see the SM [54] for further details). However, thanks to nearest-neighbor interaction and discrete translation invariance of the lattice, the Hamiltonian can be brought to a block-diagonal form in terms of the plaquette Hamiltonian H_p:

$$H_p = \frac{1}{2}\mathcal{S}_p^{\mathcal{T}} \mathcal{H}_p \mathcal{S}_p. \tag{3}$$

Here $\mathcal{H}_p$ is an orthogonal matrix-valued Hamiltonian, analogous to the second quantized Hamiltonian, whose components consist of all possible interactions between $\mathbf{S}_i$ and $\mathbf{S}_j$ for $\langle ij\rangle \in p$. However, lattice symmetries restrict the allowed finite components in $\mathcal{H}_p$, which we now consider for a square kagome lattice.

Realizations in a square kagome lattice. The square kagome lattice belongs to the dihedral (D_4) group with $n = 8$ sublattice spins, giving a 24-dimensional vector representation. Denoting the group element $\mathsf{g} \in \mathsf{D}_4$ in the $\mathcal{S}_p$ representation by the matrix-valued operators $\mathcal{D}(\mathsf{g})$, we impose the symmetry criterion that under a local symmetry transformation $\mathcal{S}_p \to \mathcal{D}(\mathsf{g})\mathcal{S}_p$ the local Hamiltonian H_p is invariant if $[\mathcal{D}(\mathsf{g}), \mathcal{H}_p] = 0$, $\forall p, \mathsf{g}$. Since local $\mathsf{O}_i(3)$ and sublattice symmetries are abandoned, the plaquette symmetry allows us to have bond- and spin-dependent interactions $J_{ij}^{\mu\nu}$ with six exchange and three DM interactions (see SM [54] for the details), leading to a bond-dependent XYZ-Heisenberg model with XY-DM interaction. However, imposing bond-independent interactions, we consider an XXZ model with DM interaction as more appropriate for realistic materials [46–48], $H = \sum_{\langle ij\rangle,\mu\nu} J^{\mu\nu} S_i^\mu S_j^\nu$. This can, for future convenience, be expressed as

$$H = J \sum_{\langle ij\rangle,\tau=\pm} \left(D^\tau e^{\mathrm{i}\tau(\Theta_i+\Theta_j)} S_i^\perp S_j^\perp + \Delta S_i^z S_j^z\right). \tag{4}$$

Here $J^{\mu\nu} = J\delta_{\mu\nu} + JD\epsilon_{\mu\nu}$, for $\mu = x$ and y, and $J^{zz} = J\Delta$, where $\delta_{\mu\nu}$ is the Kronecker delta and $\epsilon_{\mu\nu}$ is the Levi-Civita tensor. J is the exchange term, Δ is the z-axis anisotropy ratio, and JD is the XY-DM interaction strength. By diagonalizing the tensor $J^{\mu\nu}$, we define two "circularly polarized" fields: $S_i^\tau = S_i^\perp e^{\mathrm{i}\tau\Theta_i} \in \mathsf{O}_i(2) \cong \mathsf{U}_i(1)$, where $S_i^\perp = \sqrt{S^2 - (S_i^z)^2}$ is the coplanar spin magnitude and Θ_i is the azimuthal angle in the spin space, which interact via the complex (dimensionless) interaction $D^\tau = 1 + \mathrm{i}\tau D$.

Irreps in square kagome lattice. There are five conjugacy classes in this non-Abelian group, giving five irreps: $m_\alpha \equiv \mathsf{A}_{1,2}^{(d_\alpha)}$, $\mathsf{B}_{1,2}^{(d_\alpha)}$, and $\mathsf{E}^{(d_\alpha)}$, where the superscript denotes their multiplicity $(d_\alpha) = (2, 4, 3, 3, 6)$, respectively. We organize these irreps into a coplanar set, $\mathsf{m}_\perp := \{\mathsf{A}_{1,2}^{(\mathrm{a,b})}, \mathsf{B}_{1,2}^{(\mathrm{a,b})}, \mathsf{E}^{(\mathrm{a}_{x,y},\mathrm{b}_{x,y},\mathrm{c}_{x,y},\mathrm{d}_{x,y})}\}$, and an out-of-

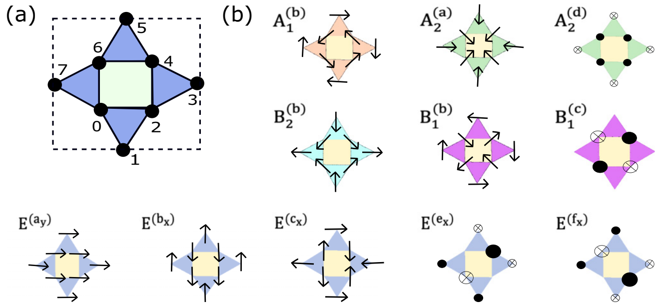

FIG. 1. (a) A plaquette of a 2D square kagome lattice, belonging to the D_4 group, is shown with sublattices enumerated as $i = 0$–7. (b) Among five irreps with different multiplets, we show a few representative irreps here, while others are shown in the Supplemental Material (SM) [54]. Each irrep consists of either $S_i^{\perp}$ (horizontal arrow) or S_i^z (open and solid dots for up and down spins) components, with the sizes of the arrows or dots dictating their magnitudes.

plane/colinear set, $\mathsf{m}_{||} := \{\mathsf{A}_2^{(\mathrm{c,d})}, \mathsf{B}_{1,2}^{(\mathrm{c})}, \mathsf{E}^{(\mathrm{e}_{x,y},\mathrm{f}_{x,y})}\}$. Representative irreps' configurations are shown in Fig. 1(b).

In the coplanar irreps $\mathsf{A}_{1,2}^{(\mathrm{a,b})}$ and $\mathsf{B}_{1,2}^{(\mathrm{a,b})}$, even/odd under C_4, the local spins S_i^{τ} are arranged in a topological texture following $\Theta_{i\in p} = Q_p\theta_i + \gamma_p$, where Θ_i and θ_i are the azimuthal angles in the spin and position manifolds, respectively. $\gamma_p \in [0, \pi)$ is the helicity angle, and $Q_p \in \pi_1(\mathbb{S}^1) \cong \mathbb{Z}$ is the topological charge. As shown in Fig. 1(b), this leads to vortices for $\mathsf{A}_{1,2}^{(\mathrm{a,b})}$ and antivortices for $\mathsf{B}_{1,2}^{(\mathrm{a,b})}$ irreps. In fact, each (anti)vortex consists of two concentric (anti)vortices in the outer and inner squares, which are not related by symmetry but interact with each other by the interaction term D^{τ}. $\mathsf{A}_1^{(\mathrm{a,b})}$ consist of concentric vortices with the same/opposite helicities ($\gamma_p = \pm\pi/2$), while $\mathsf{A}_2^{(\mathrm{a,b})}$, odd under reflection, have $\gamma_p = \pm\pi$. $\mathsf{B}_{1,2}^{(\mathrm{a,b})}$ irreps (odd under $\mathcal{C}_4$) are similar, except they contain antivortices. The out-of-plane $\mathsf{A}_2^{(\mathrm{c,d})}$ are colinear ferromagnetic (FM)/antiferromagnetic (AFM) irreps, while $\mathsf{B}_{1,2}^{(\mathrm{c})}$ are colinear AFM irreps. Finally, among the sixfold multiplets of 2D E irreps, $\mathsf{E}^{(\mathrm{a-d})}$ are coplaner FM/nematic/AFM order parameters, while $\mathsf{E}^{(\mathrm{e,f})}$ are colinear irreps. Notably, the colinear irreps $\mathsf{B}_{1,2}^{(\mathrm{c})}$ and $\mathsf{E}^{(\mathrm{e,f})}$ violate the local constraints, and hence their low-energy configurations vitiate any long-range order.

Eigenenergies. The final task is to diagonalize the multiples of the irreps. In our case, the irreps' multiplets split as either $\mathsf{O}_p(d_\alpha) = \mathsf{O}_p(2) \oplus \mathsf{O}_p(2) \oplus \cdots$ or $\mathsf{O}_p(d_\alpha) = \mathsf{O}_p(2) \oplus \mathsf{Z}_2 \oplus \cdots$, in which all $\mathsf{O}_p(2)$ operators have the same generator $\mathcal{L}_\alpha = i\sigma_y$. ϕ_α depends only on $\arg(\mathrm{D}^{\tau})$ in the eigenstates of $\mathcal{H}_p$. The resultant diagonal Hamiltonian per plaquette is

$$H_p = \sum_{\nu=1}^{3n} E_\nu |\tilde{\mathbf{m}}_\nu|^2. \tag{5}$$

Here $|\tilde{\mathbf{m}}_\nu|^2$ serves as "occupation density" to the νth energy level E_ν. Henceforth, we omit the tilde symbol for simplicity, and all irreps are considered eigenmodes unless mentioned otherwise. The functional form of E_ν in terms of J, D, and Δ is given in the SM [54]. Constrained by symmetry, $E_{\nu\in\mathsf{m}_\perp}$ depends solely on D^{τ}, while $E_{\nu\in\mathsf{m}_{||}}$ is proportional to Δ [56]. One or more irreps can form an ordered phase with a global energy minimum at NE_ν if they satisfy the constraint and frustration; otherwise, they blend with other irreps to form a degenerate ensemble, giving disordered, liquid, and mixed phases. A zero-temperature phase transition occurs at the $E_\nu = 0$ line.

Phase diagrams and correlation functions. We solve the Hamiltonian in Eq. (4) both numerically using classical MC simulations and the group theory analysis. The details of the MC simulation are given in the SM [54]. The corresponding phase diagram is summarized in Table I and shown in Fig. 2. Note that the same phase diagram is also reproduced by the lowest-energy eigenvalue E_ν, and the values of m_ν are obtained from the MC result as shown in the lower panels in Fig. 2 and agree with the group theory results.

Remarkably, we find that all the phases can be understood in terms of an analytical form of the many-body ground-state vector field as

$$\mathcal{S}_{\mathrm{GS}} = \bigoplus_p \sum_{\{\nu_p\}} m_{\nu_p} \mathcal{V}_{\nu_p}. \tag{6}$$

The ordered phase harbors a summated state of a fixed irrep $\bar{\nu} \in \{\nu_p\}$ (with $m_{\bar{\nu}} = \bar{m}$, $m_{\nu\neq\bar{\nu}} = 0$, $\forall p$); while the staggered phase features two alternating but fixed irreps $\bar{\nu}_p$ and $\bar{\nu}_q$ in neighboring plaquettes. The CSL state, on the other hand, combines an ensemble of irreps $\{\nu_p\}$ within each plaquette p. Within this ensemble, the probability amplitude m_{ν_p} may vary randomly, subject to local constraints, corresponding to the same plaquette energy. The random distribution of m_{ν_p} differs between plaquettes, resulting in an extensively degenerate ground state.

In addition, we also compare our results with a soft-spin approximation in the Fourier space [23–27], and the resulting dispersion relation is shown in the SM [54]. Given that we have experimental access to the correlation function of local spins $\mathbf{S}_{i\in p}$, we report the spin-spin correlation function. We project the structure factor $\chi(\mathbf{k}) = 1/\mathcal{N} \sum_{i,j} \langle \mathbf{S}_i \cdot \mathbf{S}_j \rangle \exp[i\mathbf{k}\cdot(\mathbf{r}_i - \mathbf{r}_j)]$ to the irreps space as

$$\langle \mathbf{S}_i \cdot \mathbf{S}_j \rangle = \sum_{\nu_p\nu_q} m_{\nu_p} m_{\nu_q} \langle \mathcal{V}_{\nu_p}^{\mathcal{T}} \mathcal{P}_i^{\mathcal{T}} \mathcal{P}_j \mathcal{V}_{\nu_q} \rangle, \tag{7}$$

with $\mathbf{r}_i$ being the ith spin's position in p and $j \in q$ plaquette.

The phase diagram in Fig. 2 reveals a predominance of (uniform or staggered) order phases in both $J < 0$ (frustration inactive) and $J > 0$ (frustration active) regions. A CSL phase emerges only at the critical line of $D \to 0$, which turns into distinct mixed/fragmented phases for $2|D|/\Delta < 1$. For $D \to 0$ and $J > 0$, three distinct CSL phases emerge with increasing Δ in Fig. 2(a) (cyan color). As $\Delta \to 0$, we have an XX model in Eq. (4), and the contributing irreps arise from the degenerate manifold of the coplanar irrep ensemble $\{m_{\nu_p}\} \subseteq \mathsf{m}_\perp$. This gives a CSL phase of $S_i^{\tau} \in \mathsf{O}_i(2)$ spins. The structure factor $\chi(\mathbf{k})$ displays a characteristic disorder pattern without any magnetic Bragg peak but with a prominent pinch-point around $\mathbf{k} = (\pm\pi, \pm3\pi)$. The pinch-point characterizes a Coloumb phase with an algebraic spin-spin correlation feature [2]. At $\Delta = 1$, the Hamiltonian is subject to a full $\mathsf{O}_i(3)$ symmetry constraint per site, resulting in symmetry-allowed access to the entire ensemble $\{m_{\nu_p}\} \subseteq \mathsf{m}_\perp \cup \mathsf{m}_{||}$. For example, $\{m_\nu\} \in \{m_{\mathsf{A}_{1,2}^{(\mathrm{a,b,c,d})}}, m_{\mathsf{B}_{1,2}^{(\mathrm{a,b})}}\}$ are

TABLE I. We tabulate all the phases and the contributing irreps obtained consistently with the MC simulation and the group theory analysis. The irrep with a bar in the third column reflects it is ordered; otherwise, it is a disordered irrep.

Phase	Acronym	Irreps $\{\nu_p\}$	Parameters	Color code
Classical spin liquid	CSL	$\mathsf{m}_{\perp} \cup \mathsf{m}_{\|\|}$	$J = 1, \Delta > 0, D = 0$	Cyan
Vortex order	VO	$\bar{\mathsf{A}}^{(a)}_{1,2}$	$J = 1, \Delta < 2D, D > 0$	Magenta
Antivortex order	AO	$\bar{\mathsf{B}}^{(a)}_{1,2}$	$J = 1, \Delta < 2D, D < 0$	Red
Fragmented AFM vortex	FAV	$\bar{\mathsf{A}}^{(a)}_{1,2} \cup \mathsf{B}^{(c)}_1$	$J = 1, \Delta > 2D, D > 0$	Black
Fragmented AFM antivortex	FAA	$\bar{\mathsf{B}}^{(a)}_{1,2} \cup \mathsf{B}^{(c)}_1$	$J = 1, \Delta > 2D, D < 0$	Black
Fragmented ferromagnet	FFM	$\bar{\mathsf{E}}^{(a)} \cup \mathsf{m}_{\|\|}$	$J = -1, \Delta > 2\|D\|, \pm D$	Black
Colinear ferromagnet order	||-FM	$\bar{\mathsf{A}}^{(c)}_2$	$\Delta J < 0, \|\Delta\| > 2\|D\|$	Green
Coplanar ferromagnet order	⊥-FM	$\bar{\mathsf{E}}^{(a)}$	$J = -1, \|\Delta\| < 2\|D\|$	Blue

degenerate at $E_\nu = -2J$ and $\{m_{\nu'}\} \in \{m_{\mathsf{B}^{(c)}_{1,2}}, m_{\mathsf{E}^{(c,d)}}\}$ are degenerate at $E_{\nu'} = -4J$, making a larger CSL ensemble degenerate at energy $E_p = m_\nu^2 E_\nu + m_{\nu'}^2 E_{\nu'} = -4J$ for $m_\nu = \sqrt{2} m_{\nu'}$. Consequently, $\chi(\mathbf{k})$ displays pinch-point correlations among both S_i^τ and S_i^z. Finally, as $\Delta \to \infty$, the Hamiltonian [last term in Eq. (4)] retains a residual local Z_2 symmetry constraint, and the disordered ground state solely stems from the $\{m_{\nu_p}\} \subseteq \mathsf{m}_{||}$ ensemble. $\chi(\mathbf{k})$ is contributed solely by S_i^z with pinch-points at $\mathbf{k} = (\pm\pi, \pm 3\pi)$. Based on their distinct local constraints, it is convenient to refer to these phases as $\mathsf{O}(2)$, $\mathsf{O}(3)$, and Z_2 CSLs, respectively, without implying a Landau-type phase boundary between them.

Any finite D steers the CSL phase into either ordered or fragmented (mixed) phases. Note that vortex irreps $\mathsf{A}_1^{(a,b)}$ and $\mathsf{A}_2^{(a,b)}$ are degenerate at $E_\nu = 2D \pm 2\sqrt{D^2 + (1+D)^2}$, while the antivortex irreps $\mathsf{B}_1^{(a,b)}$ and $\mathsf{B}_2^{(a,b)}$ are degenerate at $E_\nu = -2D \pm 2\sqrt{D^2 + (1-D)^2}$. This makes all the phases in Figs. 2(a) and 2(b) symmetric for $D \leftrightarrow -D$ with vortices $\leftrightarrow$ antivortices. Hence, we mainly focus on the $-D$ region with antivortices for the discussions.

For weak out-of-plane anisotropy $\Delta < 2|D|$, we have ordered phases of (anti)vortices for $\mp D$, which we call antivortex order/vortex order (AO/VO) phases (red/magenta regions in Fig. 2). In the AO phase, the degenerate irreps $\mathsf{B}^{(a)}_{1,2}$ are mixed in an $\mathsf{O}(2)$ order parameter and are staggered between the neighboring plaquettes with a $\gamma_p = \pi$ phase shift. The extracted values of the order parameter m from the MC data confirm the only finite and uniform weight of the $\bar{m}_{\mathsf{B}^{(a)}_{1,2}}$ irreps in the AO phase, as shown in Fig. 2(d) (lower panel). The ordering is also evident in $\chi(\mathbf{k})$ with a magnetic Bragg peak at $\mathbf{k} = (\pi, \pi)$. Interestingly, the CSL lies at the phase transition line between the VO and AO phases.

However, for strong $\Delta > 2|D|$ (with AFM anisotropy $J\Delta > 0$), the coplanar ordered irreps become scrambled with disordered out-of-plane irreps: $\{m_{\nu_p}\}_{\rm mix} \subseteq \bar{m}_{\mathsf{A/B}} \cup \mathsf{m}_{||}$, in the black region in Fig. 2(a). In particular, the outer (anti)vortex maintains coplanarity, while the inner (anti)vortex mixes with the $m_{\mathsf{B}^{(c)}_1} \in \mathsf{m}_{||}$ irrep. The combination produces a novel *AFM vortex/AFM antivortex* texture within the inner square where neighboring spins possess opposite easy axes [57]. Consequently, $\mathbf{S}_i$ spin fragments into its S_i^z components, which become noninteracting and fail to order or exhibit any significant correlation, while the S_i^τ fields exhibit long-range order with magnetic Bragg peaks in the structure factor [see Figs. 3(b) and 3(c)]. We denote these phases as fragmented AFM vortex (FAV) and fragmented AFM antivortex (FAA)

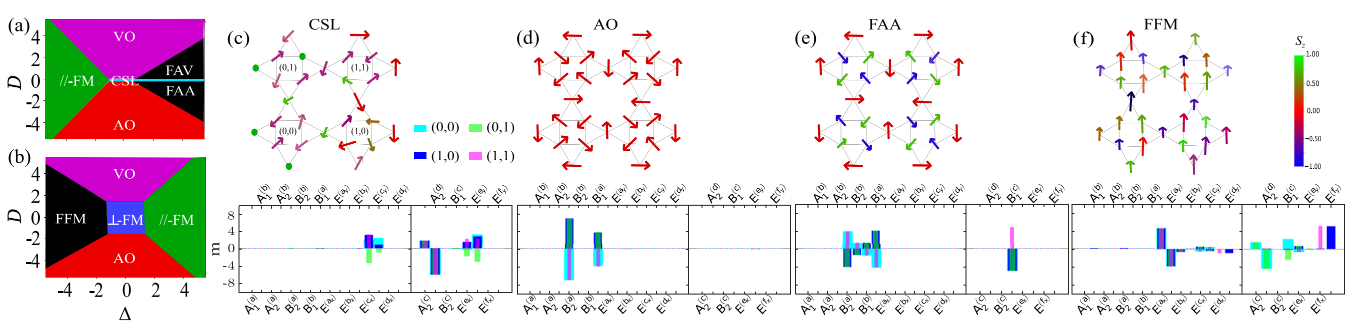

FIG. 2. Computed phase diagrams within the MC simulation (also group theory analysis) are shown for (a) AFM ($J = +1$) and (b) FM ($J = -1$) couplings. We highlight spin textures in a randomly chosen four-plaquette setting for representative phases (upper panels) and respective ensembles of irreps in four plaquettes (lower panels). (c) CSL at $(J, \Delta, D) = (1, 1, 0)$ showing disordered values of m_ν from both in-plane and out-of-plane ensembles. (d) Antivortex order (AO) at $(1, 0, -3)$ where degenerate irreps $\mathsf{B}^{(a)}_{1,2}$ are staggered. (e) FAA phase at $(1, 4, -1)$ where $\mathsf{B}^{(a)}_{1,2}$ are ordered but $\mathsf{B}^{(c)}_1$ is disordered. (f) FFM phase at $(-1, -2.5, 0)$ where 2D irrep $\mathsf{E}^{(a)}$ is ferromagnetically ordered in-plane, but out-of-plane irreps are disordered. Note that all disordered values take random numbers between different plaquettes, while we display only four representative plaquettes here.

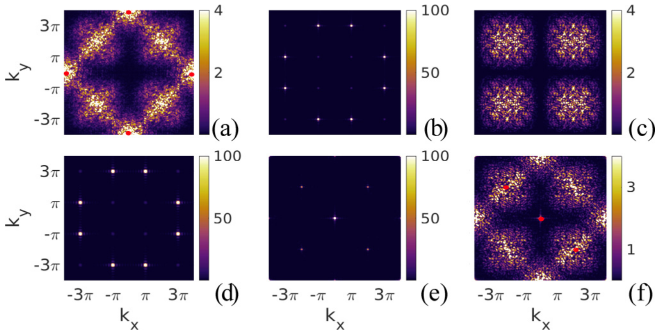

FIG. 3. Simulated $\chi(\mathbf{k})$ is plotted in the momentum space for the four phases discussed in Fig. 2. (a) CSL at $(J, \Delta, D) = (1, 1, 0)$, where red dots are plotted separately to signify additional strong magnetic Bragg-like peaks that overwhelm the spectral density of the disordered pattern. (b), (c) FFA at $(1, 4, -1)$ where the plots for the ordered $S_i^{\perp}$ and disordered S_i^z components are separated in panels (b) and (c), respectively. (d) AO at $(1, 0, -3)$ showing Bragg peaks similar to $S_i^{\perp}$ components in panel (b). (e), (f) FFM phase at $(-1, -2.5, 0)$ with FM ordered $S_i^{\perp}$ and disordered S_i^z are separated in panels (e) and (f). Panels (a) and (f) host pinch-points around $(\pi, 3\pi)$ and its equivalent points.

for $\pm D$ regions and confirm the same values of m_ν from the MC result.

For strong $\Delta > 2|D|$ with FM anisotropy, $\Delta < 0$ and $J > 0$ naturally select colinear FM order of the $\mathsf{A}_2^{(c)}$ irrep [green region Fig. 2(a)]. We denote this phase as $||-$FM. The same phase reemerges for $\Delta > 0$ and $J < 0$ in Fig. 2(b).

The interplay between the FM interaction, $J = -1$, and the strong AFM anisotropy, $\Delta > 2|D|$, generates a distinct fragmented phase [see Fig. 2(b) (black region)]. The extracted values of m from the MC data show that the in-plane FM 2D irrep $\bar{m}_{\mathsf{E}^{(a)}}$ is ordered while the out-of-plane AFM irreps $\in m_{||}$ are disordered [see Fig. 2(f)]. These out-of-plane irreps violate the local constraint, leading to an intriguing fragmented structure in $\chi(\mathbf{k})$, resulting in an in-plane FM order in S_i^{τ}, but a pinch-point disorder in S_i^z [see Figs. 3(e) and 3(f)]. We dub this a fragmented FM (FFM) phase.

Any finite D disfavors this mixed phase, causing a phase transition at $D > 2\Delta$ to in-plane VO or AO orders for $\pm D$, as observed in the $J = 1$ phase diagram. The remaining two phases are readily identifiable: a uniform coplanar FM (namely, $\perp$-FM) order with an $\bar{m}_{\mathsf{E}^{(a)}}$ irrep at $\Delta \to 0$ [blue region in Fig. 2(b)], and an out-of-plane $||$-FM order with $\bar{m}_{\mathsf{A}_2^{(c)}}$ for $J\Delta \to \infty$ [green region in Fig. 2(b)].

Conclusions and outlook. Discussions on the excitations and phase transitions of VO/AO phases are merited. The VO/AO phases (red and magenta) exhibit novel collective excitations. Gapless collective excitations emerge from the long-wavelength fluctuation of the helicity angle γ_p across the lattice, protected by the topology of the irreps' space through the charge $Q_p \in \mathbb{Z}$. These modes, termed helicity phase modes or phasons, possess novel characteristics. The two concentric vortices per plaquette are coupled by interaction but not symmetry. Frustration affects only the outer vortex, resulting in the fragmentation of the excitation spectrum into a collective mode for the ordered fields and local excitations for the disordered components. The Mermin-Wagner theorem dictates the instability of ordered states to gapless magnons or phason modes, while disordered phases tend to order via thermal fluctuations according to the order-by-disorder paradigm [14,16–18]. Moreover, the VO/AO phases for $\pm D$ consist of different irreps, i.e., distinct conjugacy classes, that do not couple in the Hamiltonian. Hence, their phase boundary at $D = 0$ signifies a topological phase transition associated with a spin liquid phase at the critical point, reminiscent of the deconfined critical point [58]. The CSL critical point can be extended by applying a magnetic field in the z direction (see the SM [54]). Finally, transitions between ordered and fragmented phases, or within fragmented phases, offer intriguing avenues for studying non-Landau-type phase transitions.

Acknowledgments. We thank Shivaji Sondhi for useful discussions. T.D. acknowledges research funding from the S.E.R.B. Department of Science and Technology, India, under Core Research Grant (CRG) Grant No. CRG/2022/00341, and acknowledges the computational facility at S.E.R.C. Param Pravega under NSM Grant No. DST/NSM/R&D HPC Applications/2021/39.

[1] L. Balents, Nature (London) **464**, 199 (2010).
[2] C. L. Henley, Annu. Rev. Condens. Matter Phys. **1**, 179 (2010).
[3] R. Moessner and J. T. Chalker, Phys. Rev. Lett. **80**, 2929 (1998).
[4] J. Rehn, A. Sen, K. Damle, and R. Moessner, Phys. Rev. Lett. **117**, 167201 (2016).
[5] O. Benton, L. Jaubert, H. Yan, and N. Shannon, Nat. Commun. **7**, 11572 (2016).
[6] O. Benton and R. Moessner, Phys. Rev. Lett. **127**, 107202 (2021).
[7] C. Castelnovo, R. Moessner, and S. Sondhi, Annu. Rev. Condens. Matter Phys. **3**, 35 (2012).
[8] C. Nisoli, R. Moessner, and P. Schiffer, Rev. Mod. Phys. **85**, 1473 (2013).
[9] K. A. Ross, L. Savary, B. D. Gaulin, and L. Balents, Phys. Rev. X **1**, 021002 (2011).
[10] M. E. Brooks-Bartlett, S. T. Banks, L. D. C. Jaubert, A. Harman-Clarke, and P. C. W. Holdsworth, Phys. Rev. X **4**, 011007 (2014).
[11] S. Powell, Phys. Rev. B **91**, 094431 (2015).
[12] S. Petit, E. Lhotel, B. Canals, M. Ciomaga-Hatnean, J. Ollivier, H. Mutka, E. Ressouche, A. R. Wildes, M. R. Lees, and G. Balakrishnan, Nat. Phys. **12**, 746 (2016).
[13] B. Canals, I.-A. Chioar, V.-D. Nguyen, M. Hehn, D. Lacour, F. Montaigne, A. Locatelli, T. O. Mentes, B. S. Burgos, and N. Rougemaille, Nat. Commun. **7**, 11446 (2016).
[14] J. Villain, R. Bidaux, J.-P. Carton, and R. Conte, J. Phys. (Fr.) **41**, 1263 (1980).
[15] C. L. Henley, Phys. Rev. Lett. **62**, 2056 (1989).
[16] P. Chandra, P. Coleman, and A. I. Larkin, Phys. Rev. Lett. **64**, 88 (1990).

[17] J. T. Chalker, P. C. W. Holdsworth, and E. F. Shender, Phys. Rev. Lett. **68**, 855 (1992).
[18] E. F. Shender and P. C. W. Holdsworth, Order by disorder and topology in frustrated magnetic systems, in *Fluctuations and Order: The New Synthesis*, edited by M. Millonas (Springer, New York, 1996), pp. 259–279.
[19] M. Biskup, L. Chayes, and S. A. Kivelson, Ann. Henri Poincaré **5**, 1181 (2004).
[20] A. Pizzi, A. Nunnenkamp, and J. Knolle, Phys. Rev. Lett. **127**, 140602 (2021).
[21] B. Placke, O. Benton, and R. Moessner, Phys. Rev. B **110**, L020401 (2024).
[22] D. Dahlbom, H. Zhang, Z. Laraib, D. M. Pajerowski, K. Barros, and C. Batista, arXiv:2304.03874.
[23] R. P. Nutakki, L. D. C. Jaubert, and L. Pollet, SciPost Phys. **15**, 040 (2023).
[24] N. Davier, F. A. Gómez Albarracín, H. D. Rosales, and P. Pujol, Phys. Rev. B **108**, 054408 (2023).
[25] H. Yan, O. Benton, R. Moessner, and A. H. Nevidomskyy, arXiv:2305.00155.
[26] H. Yan, O. Benton, A. H. Nevidomskyy, and R. Moessner, arXiv:2305.19189.
[27] Y. Fang, J. Cano, A. H. Nevidomskyy, and H. Yan, arXiv:2309.12652.
[28] Z. Nussinov, Phys. Rev. B **69**, 014208 (2004).
[29] Z. Nussinov, arXiv:cond-mat/0105253.
[30] S. T. Bramwell, Philos. Trans. R. Soc. London A **370**, 5738 (2012).
[31] L. Savary and L. Balents, Phys. Rev. Lett. **108**, 037202 (2012).
[32] R. Siddharthan, B. S. Shastry, A. P. Ramirez, A. Hayashi, R. J. Cava, and S. Rosenkranz, Phys. Rev. Lett. **83**, 1854 (1999).
[33] S. T. Bramwell and M. J. P. Gingras, Science **294**, 1495 (2001).
[34] S. V. Isakov, K. Gregor, R. Moessner, and S. L. Sondhi, Phys. Rev. Lett. **93**, 167204 (2004).
[35] H. Yan, O. Benton, L. Jaubert, and N. Shannon, Phys. Rev. B **95**, 094422 (2017).
[36] P. H. Conlon and J. T. Chalker, Phys. Rev. Lett. **102**, 237206 (2009).
[37] P. H. Conlon and J. T. Chalker, Phys. Rev. B **81**, 224413 (2010).
[38] L. A. S. Mól, A. R. Pereira, and W. A. Moura-Melo, Phys. Rev. B **85**, 184410 (2012).
[39] Y. Li, P. Gegenwart, and A. A. Tsirlin, J. Phys.: Condens. Matter **32**, 224004 (2020).
[40] D. T. Liu, F. J. Burnell, L. D. C. Jaubert, and J. T. Chalker, Phys. Rev. B **94**, 224413 (2016).
[41] Y. Iqbal, H. O. Jeschke, J. Reuther, R. Valentí, I. I. Mazin, M. Greiter, and R. Thomale, Phys. Rev. B **92**, 220404(R) (2015).
[42] T. Mizoguchi, L. D. C. Jaubert, and M. Udagawa, Phys. Rev. Lett. **119**, 077207 (2017).
[43] K. Essafi, O. Benton, and L. D. C. Jaubert, Phys. Rev. B **96**, 205126 (2017).
[44] T. Yildirim, A. B. Harris, and E. F. Shender, Phys. Rev. B **58**, 3144 (1998).
[45] J. Rehn, A. Sen, and R. Moessner, Phys. Rev. Lett. **118**, 047201 (2017).
[46] M. Fujihala, K. Morita, R. Mole, S. Mitsuda, T. Tohyama, S.-i. Yano, D. Yu, S. Sota, T. Kuwai, A. Koda *et al.*, Nat. Commun. **11**, 3429 (2020).
[47] O. V. Yakubovich, L. V. Shvanskaya, G. V. Kiriukhina, A. S. Volkov, O. V. Dimitrova, and A. N. Vasiliev, Inorg. Chem. **60**, 11450 (2021).
[48] M. M. Markina, P. S. Berdonosov, T. M. Vasilchikova, K. V. Zakharov, A. F. Murtazoev, V. A. Dolgikh, A. V. Moskin, V. N. Glazkov, A. I. Smirnov, and A. N. Vasiliev, Mater. Chem. Phys. **319**, 129348 (2024).
[49] N. Astrakhantsev, F. Ferrari, N. Niggemann, T. Müller, A. Chauhan, A. Kshetrimayum, P. Ghosh, N. Regnault, R. Thomale, J. Reuther, T. Neupert, and Y. Iqbal, Phys. Rev. B **104**, L220408 (2021).
[50] J. Richter, O. Derzhko, and J. Schnack, Phys. Rev. B **105**, 144427 (2022).
[51] N. Niggemann, N. Astrakhantsev, A. Ralko, F. Ferrari, A. Maity, T. Müller, J. Richter, R. Thomale, T. Neupert, J. Reuther, Y. Iqbal, and H. O. Jeschke, Phys. Rev. B **108**, L241117 (2023).
[52] J. Richter and J. Schnack, Phys. Rev. B **107**, 245115 (2023).
[53] M. Gembé, H.-J. Schmidt, C. Hickey, J. Richter, Y. Iqbal, and S. Trebst, Phys. Rev. Res. **5**, 043204 (2023).
[54] See Supplemental Material at http://link.aps.org/supplemental/10.1103/PhysRevB.110.L060401 for the details of the calculations and results.
[55] We define in the SM [54] the operation $\mathcal{T}$ for the dual vector as transpose T followed by a normalization factor of 6/8 to adjust the length of the plaquette spin to be $|\mathcal{S}_p| = 6$.
[56] Specifically, the (anti-)vortex irreps $\mathsf{B}_{1,2}^{(\mathrm{a,b})}$ and $\mathsf{A}_{1,2}^{(\mathrm{a,b})}$ are promoted by $\mp D$, while $\mathsf{E}^{(\mathrm{a,b})}$ do not depend on D.
[57] This AFM-vortex topology is homotopically distinct from the known AFM skyrmion [59] and has not been predicted previously.
[58] T. Senthil, A. Vishwanath, L. Balents, S. Sachdev, and M. P. A. Fisher, Science **303**, 1490 (2004).
[59] X. Zhang, Y. Zhou, and M. Ezawa, Sci. Rep. **6**, 24795 (2016).